

Velocity statistics from spectral line data: effects of density-velocity correlations, magnetic field, and shear

A. Esquivel,¹*, A. Lazarian,¹*, D. Pogosyan,² J. Cho¹*

¹*Astronomy Department, University of Wisconsin-Madison, 475 N. Charter St., Madison, WI 53706, USA*

²*Department of Physics, University of Alberta, Edmonton, Alberta T6G 2J1, Canada*

Draft Version 7 February 2020

ABSTRACT

In a previous work Lazarian and Pogosyan suggested a technique to extract velocity and density statistics, of interstellar turbulence, by means of analysing statistics of spectral line data cubes. In this paper we test that technique, by studying the effect of correlation between velocity and density fields, providing a systematic analysis of the noise, and exploring the effect of a linear shear. We make use of both compressible MHD simulations and synthetic data to emulate spectroscopic observations. With such synthetic spectroscopic data, we studied anisotropies of the two point statistics and related those anisotropies with the magnetic field direction. This presents a new technique for magnetic field studies. The results show that the velocity and density spectral indices measured are consistent with the analytical predictions. We identified the dominant source of error with the limited number of data points along a given line of sight. We argue that in real observations the number of emitting elements is essentially infinite and that source of noise vanishes.

Key words: turbulence – ISM: general, structure – MHD – radio lines: MHD.

1 INTRODUCTION

The very large Reynolds numbers (defined as the ratio of the inertial force to the viscous force acting on a parcel of gas) clearly suggest that the interstellar medium is turbulent. Understanding of this turbulence is crucial to the correct and complete description of many physical processes that take place in the ISM: molecular cloud dynamics, star formation, heat transfer, magnetic reconnection, accretion disks, cosmic ray propagation and diffusion, just to mention a few.

To adequately describe turbulence we need to use statistical methods, to extract the underlying regularities and reject incidental details. So far, studies of turbulence statistics have been most successful using interstellar scintillations, and have provided important information of the density statistics on scales $10^8 - 10^5 \text{ cm}$, (see Narayan & Goodman 1989; Spangler & Gwinn 1990). These studies are done with the ionised media, and are restricted to the density fluctuations. We expect to observe power-law power spectrum of density in a turbulent medium. However, the distribution of sizes of sand grains in a beach follows a power-law but it is not turbulence. Power-law density statistics fails to distinguish between fossil and active turbulence. Therefore would be better to study a more direct statistic: velocity fluctuations. Studies of the neutral media have included velocity information, e.g. using spectral line widths, centroids of velocity (Miesch & Bally 1994; Scalo 1987);

or more fancy statistics (Heyer & Schloerb 1997; Rosolowsky et al. 1999; Brunt & Heyer 2002a,b). A discussion of various approaches to the study of turbulence with spectral line data can be found in Lazarian (1999). In particular the problem of the contribution of velocity and density fluctuations to the emissivity statistics was addressed in Lazarian & Pogosyan (2000, hereafter LP00), where analytical description of the power spectrum of the emissivity in velocity channels was obtained. This study provides us with a technique to extract the spectral indices of density and velocity from spectral line data cubes. H I was chosen as a test case because it was possible to disregard self-absorption and consider the emissivity going as the first power of the density. The technique, termed as velocity-channel analysis (or simply, VCA), studies variations of the power spectra in velocity channels with velocity resolution. Predictions of the spectral index variation of LP00 have been confirmed through observations (Stanimirović & Lazarian 2001), and with the aid of numerical simulations (Lazarian et al. 2001). The first tests using numerical data (Lazarian et al. 2001) were satisfactory, however they did not address the problems of noise, effects of magnetic field and galactic shear; and the study of velocity-density correlations was performed over a very limited dynamical range.

In this work we test the predictions in LP00, we systematically analyse the effects of velocity-density correlations, unlike Lazarian et al. (2001) we include a study of the effect of shear, and address the issue of an anisotropic turbulent cascade, with their implications on the VCA. We also subject the sources of noise to scrutiny.

In §2 we review the basic problem, we then (§3) test the extraction of the spectral indices using the VCA, and the density-

* E-mail: esquivel@astro.wisc.edu; lazarian@astro.wisc.edu; pogosyan@phys.ualberta.ca; cho@astro.wisc.edu

velocity correlations. In §4 we study the effect of shear in the VCA. The anisotropic cascade, and a possible new method to extract information of the magnetic field direction can be found in §5. And we finally provide a summary of our results (§6).

2 STATISTICS OF SPECTRAL LINE DATA AND VCA

Spectral line observations contain important information of density and velocity. The problem is that both velocity fluctuations and density fluctuations contribute to the intensity of a spectral line at a given velocity, and their separation is far from trivial.

2.1 3D turbulence statistics

Turbulence, due to its stochastic nature is studied using statistical tools, such as 3D correlation and structure functions (see Monin & Yaglom 1975). For instance, the density correlation function can be expressed as

$$\xi(\mathbf{r}) = \langle \rho(\mathbf{x})\rho(\mathbf{x} + \mathbf{r}) \rangle, \quad (1)$$

where \mathbf{x} is the spatial position (xyz in Cartesian coordinates), \mathbf{r} is the spatial separation (or ‘lag’), and the average is to be performed over all \mathbf{x} space. The power spectrum provides an alternative description and is related to the correlation function (CF) as

$$P(\mathbf{k}) = \int d\mathbf{r} e^{i\mathbf{k} \cdot \mathbf{r}} \xi(\mathbf{r}), \quad (2)$$

where \mathbf{k} is the wave-number, related to the scale under study like $k = 2\pi/r$, and the integration is performed over all 3D space. For power-law statistics, the N dimensional power spectrum $P_N \sim k^n$ and the correlation $\xi_N \sim r^{-\gamma}$ have indices related as $n = -N + \gamma$, in other words

$$(\text{spectral index}) = (-\text{spatial dimensions} + \text{CF index}). \quad (3)$$

2.2 Statistics in position-position-velocity (PPV) space

In spectroscopic observations, we don’t observe the gas distribution in real space coordinates $\mathbf{x} \equiv (x, y, z)$. Instead the intensity of the emission in a given spectral line is measured towards some direction in the sky, given by $\mathbf{X} \equiv (x, y)$, and at a given line-of-sight (LOS) velocity v . Thus, the coordinates of observational PPV cubes are (\mathbf{X}, v) . If we identify the z coordinate with the LOS, then the relation between the real space and PPV descriptions is that of a map $(\mathbf{X}, z) \rightarrow (\mathbf{X}, v)$.

At a given position \mathbf{x} the LOS component of the velocity v can be decomposed as a regular flow velocity $v_{reg}(\mathbf{x})$, plus a thermal component $v_{thermal}$ and a turbulent component $u(\mathbf{x})$ so that the observed Doppler shifted atoms follow a Maxwellian distribution

$$\phi_v(\mathbf{x})dv = \frac{1}{(2\pi\beta)^{1/2}} \exp \left\{ -\frac{[v - v_{reg}(\mathbf{x}) - u(\mathbf{x})]^2}{2\beta} \right\} dv, \quad (4)$$

where $\beta = \kappa_B T/m$, m is the atomic mass, T the gas temperature, and κ_B the Maxwell-Boltzmann constant.

The density of emitters in PPV space $\rho_s(\mathbf{X}, v)$ can be obtained by integration along the LOS:

$$\rho_s(\mathbf{X}, v)d\mathbf{X}dv = \left[\int dz \rho(\mathbf{x})\phi(\mathbf{x}) \right] d\mathbf{X}dv, \quad (5)$$

where $\rho(\mathbf{x})$ is the mass density of the gas in spatial coordinates. This expression just counts the number of atoms along the LOS, at a given position \mathbf{X} with a z component of velocity in the interval $[v, v + dv]$, and the limits of integration are defined by the extent of spatial distribution of emitting gas.

The statistics available in PPV are the correlation functions $\xi_s \equiv \langle \rho_s(\mathbf{X}_1, v_1)\rho_s(\mathbf{X}_2, v_2) \rangle$ and the power spectra (this can be 1D, 2D or 3D) of emissivity fluctuations. Relations between this statistics and the underlying velocity and density spectra were established in LP00, where the 2D power spectrum in velocity channels was used. This spectrum can be directly obtained with radio-interferometric observations (see Lazarian 1995).

2.3 Velocity-channel analysis (VCA)

This technique was developed in LP00 to extract the velocity and density spectral indices of turbulence from spectral line data. LP00 provides analytical predictions for the emissivity power spectral indices in velocity channels, as a function of the velocity resolution employed. The relative contribution to the intensity in a velocity channel (also referred as ‘slice’) to the total fluctuations of intensity, changes in a regular fashion with the width of the velocity slice. This is easy to understand qualitatively since more velocity fluctuations within a channel are averaged out as we increase the thickness of the channel, decreasing the relative contribution of velocity. If the 3D density power spectrum is $P_n \propto k^n$, two distinct regimes are present when: (a) $n > -3$, and (b) $n < -3$. A summary of the predictions in LP00 for the intensity spectral index in 2D velocity channels is given in Table 1. In both cases (shallow or steep density) the power-law index *gradually steepens* with the increase of the velocity slice thickness. In the thickest velocity channels all the velocity information is averaged out and we naturally get the density spectral index n . The velocity fluctuations, with a 3D velocity power spectrum $P_v \sim k^{-3-m/2}$, dominate in thin channels. For $n < -3$ all the structure seen in the velocity channels is actually due to velocity fluctuations, this immediately sends a warning against identifying structures in PPV as actual density enhancements (‘clouds’). The spectral velocity index is¹

$$\mu = -3 - \frac{m}{2}, \quad (6)$$

it can be obtained if we know the density velocity index and find the index m in thin channels. Note, that the notion of thin and thick slices depends on the turbulence scale under study, and the same slice can be thick for small scale turbulent fluctuations and thin for large scale ones. The formal criterion for the slice to be thick is that *the dispersion of turbulent velocities on the scale studied should be less than the velocity slice thickness*. Otherwise the slice is *thin*. In following sections we perform tests of the VCA using numerical data, and take a step further exploring the sources of uncertainty and the effects of shear in the VCA.

¹ One may observe that the spectrum of fluctuations within a slice decreases as the spectrum of velocity steepens. This can be understood qualitatively if one takes into account that larger velocity dispersion, at a particular scale, means a distribution of emitting atoms over a large phase volume. As the result the number of emitters within a velocity channels decreases.

Table 1. A summary of analytical results derived in LP00.

Slice thickness	Shallow 3-D density $P_n \propto k^n, n > -3$	Steep 3-D density $P_n \propto k^n, n < -3$
2-D intensity spectrum for thin ^a slice	$\propto k^{n+m/2}$	$\propto k^{-3+m/2}$
2-D intensity spectrum for thick ^b slice	$\propto k^n$	$\propto k^{-3-m/2}$
2-D intensity spectrum for very thick ^c slice	$\propto k^n$	$\propto k^n$

^a channel width < velocity dispersion at the scale under study

^b channel width > velocity dispersion at the scale under study

^c substantial part of the velocity profile is integrated over

3 TESTING THE VCA

Numerical simulations provide good means of theory testing. Using numerical data, we can measure directly the velocity and density statistics. With the same data we can produce synthetic spectra, and analyse them as an observer would do. However we need to be aware of the differences of synthetic and real data. For instance, only limited number of points is available with numerics. This, as we show later, results in noise.

3.1 The data

Along the paper we make use of three types of data to construct the PPV cubes and analyse the power spectrum.

(i) MHD simulations. We use a 3rd-order hybrid essentially-non-oscillatory (ENO) code to simulate fully developed turbulence. It was performed on a 216^3 Cartesian grid it is isothermal, compressible, and with a mean magnetic field in the x direction. To reduce spurious oscillations near shocks, we combine two ENO schemes. When variables are sufficiently smooth, we use the 3rd-order weighted ENO scheme (Jiang & Hu 1999) without characteristic mode decomposition. When opposite is true, we use the 3rd-order Convex ENO scheme (Liu & Osher 1998). We use a three-stage Runge-Kutta method for time integration. We solve the ideal MHD equations in a periodic box:

$$\begin{aligned} \frac{\partial \rho}{\partial t} + \nabla \cdot (\rho \mathbf{v}) &= 0, \\ \frac{\partial \mathbf{v}}{\partial t} + \mathbf{v} \cdot \nabla \mathbf{v} + \rho^{-1} \nabla (a^2 \rho) - (\nabla \times \mathbf{B}) \times \mathbf{B} / 4\pi\rho &= \mathbf{f}, \quad (7) \\ \frac{\partial \mathbf{B}}{\partial t} - \nabla \times (\mathbf{v} \times \mathbf{B}) &= 0, \end{aligned}$$

with $\nabla \cdot \mathbf{B} = 0$ and we use an isothermal equation of state. Here \mathbf{f} is a random large-scale driving force, ρ is density, \mathbf{v} is the velocity, and \mathbf{B} is magnetic field. The rms velocity δV is maintained to be approximately unity, so that \mathbf{v} can be viewed as the velocity measured in units of the rms velocity of the system, and $B/\sqrt{4\pi\rho}$ as the Alfvén speed in the same units. The time t is roughly in units of the large eddy turnover time ($\sim L/\delta V$) and the length in units of L , the scale of the energy injection. The magnetic field consists of the uniform background field and a fluctuating field: $\mathbf{B} = \mathbf{B}_0 + \mathbf{b}$. The Alfvén velocity of the mean field is roughly the same as the rms velocity. The average Mach number is ~ 2.5 .

The output is the density and the velocity fields. The PPV cubes constructed with this data have a correlation between the velocity and the density fields which is self-consistent with MHD evolution, and are used to test the applicability of the VCA where the basic assumption was to disregard such correlation.

(ii) ‘Modified’ data. Due to numerical limitations, the power spectrum of the simulations mentioned above doesn’t show exact power-law behaviour over the desired inertial range, therefore making difficult to test the VCA, which deals with power-law spectra. For that reason we apply the same procedure as in Lazarian et al. (2001) to modify the power spectrum to follow a power-law preserving most of the phase correlations. The procedure consists in replacing the amplitudes of the Fourier transform of the data so they follow a power-law while keeping the phases intact (were most of the spatial information is). The set of simulations used here show a larger well-developed inertial range than those in Lazarian et al. (2001); therefore the ‘correction’ introduced, at least for the $-11/3$ index case, is smaller.

(iii) Gaussian fields. We use a standard procedure to generate Gaussian fields with prescribed power-law spectrum (see Bond, Kofman & Pogosyan 1996). We generate a Fourier representation of the field

$$F(k) = \sum k a_k P(k)^{1/2} e^{ikr}, \quad (8)$$

where a_k are independent Gaussian variables with dispersion 1, and a mean of 0 for velocity fields or 1 for density fields; in our notation the wave-number $k = 2\pi L/\lambda$, where λ is the wavelength associated with k , and L is the box size. Then to obtain the field in configuration space a Fourier transform is applied. Velocity and density fields generated this way are entirely uncorrelated. However the facility of generating as many cubes as we want in a short amount of time is very useful to improve our statistical sample.

Comparing (ii) and (iii) allows to test the importance of density-velocity correlations.

With the data cubes mentioned above we produced synthetic spectra (i.e. PPV ‘cubes’ –although strictly speaking they are parallelepipeds as the sizes need not to be the same in all directions–) to analyse them using VCA. To construct the PPV cubes we use the following procedure. We generate a matrix of the same dimensions in \mathbf{X} as the x data and a given number of velocity bins (velocity channels) as the third dimension. The velocity bins are equally spaced ranging from the minimum value of the velocity (v_{min}) to the maximum value of the velocity (v_{max}) in the whole velocity data cube. We then sum all the elements of the density cube in a position \mathbf{X} that correspond to each velocity bin. This way we are simulating observational data, neglecting self absorption, and assuming that the thermal width of the emitting gas is always smaller than the thickness of the velocity channels.

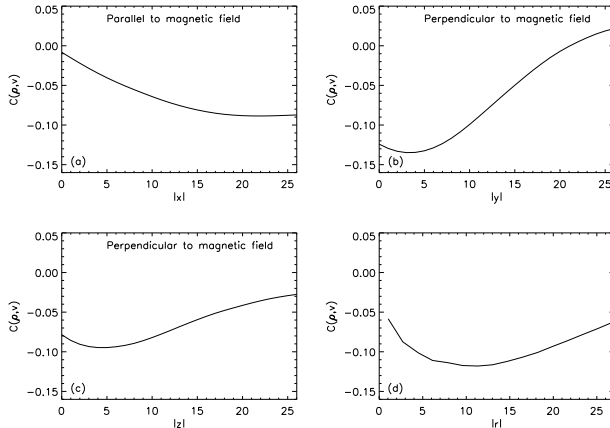


Figure 1. Correlation of the density and velocity fields. (a) the average projection of the cross-correlation on the x axis (parallel to the mean magnetic field), (b) the average projection of the correlation on the y axis (perpendicular to the mean magnetic field), (c) the average projection of the correlation on the z axis (perpendicular to the mean magnetic field), and (d) average projection of the correlation and the spatial separation r .

3.2 Density and velocity correlations

The principal assumption made in LP00 was to consider the density and velocity field as uncorrelated. We computed the correlation of the density and the velocity fields as

$$C(r) = \frac{\langle \rho(\mathbf{x}) \mathbf{u}(\mathbf{x} + \mathbf{r}) \cdot \mathbf{r} / |\mathbf{r}| \rangle}{\sigma_\rho \sigma_u}. \quad (9)$$

Where \mathbf{r} is the spatial separation ('lag'), \mathbf{x} is the spatial position, ρ the density field, \mathbf{u} is the velocity field, σ_ρ and σ_u are the standard deviations of the density and velocity fields respectively. The average is to be performed over all \mathbf{x} space and angles of \mathbf{r} . For numerical economy Lazarian et al. (2001) used Fourier transform techniques to obtain similar information (although restricted to the LOS velocity component). Here this is done directly using equation (9), which is applied to the original output from the MHD simulations. We found moderate correlations, the maximum correlation (in absolute value) was of ~ 0.22 . This correlation is shown in Fig. 1, where we plotted the average projection of the cross-correlation on the x , y , z axis and the average magnitude of the separation r . Clearly the velocity and density correlations are very different along and perpendicular to the magnetic field direction.

3.3 Applying the VCA

In this subsection we used the output of the MHD simulations and modified the spectral indices as mentioned before. We created a density data cube with spectral index modified to $-11/3$, and LOS velocity cubes with indices of -3.1 , -3.3 , -3.5 , $-11/3$ (Kolmogorov), -3.8 , and -4.0 . With each of those velocity and the density cubes we constructed PPV cubes with different velocity resolutions, corresponding to 150, 100, 75, 50, 25, 15, 10, 6, 4, 2, and 1 number of channels. The power spectra in velocity channels (averaged over all velocity channels for each PPV cube) is presented in Fig. 2.

We should note, that whether a slice in velocity space can be considered *thin* or *thick* depends not only on the slice width $\delta v = (v_{max} - v_{min})/N = \Delta v/N$, where N is the number of channels, but on the scale as well. For power-law statistics the

Table 2. Measured emissivity spectral indices of Fig. 2

Num. of channels	Predicted spectral index (γ)					
	-2.95	-2.85	-2.75	-2.67	-2.6	-2.5
	Velocity index (μ)					
150	-2.27	-2.25	-2.22	-2.19	-2.18	-2.15
100	-2.30	-2.27	-2.15	-2.22	-2.20	-2.18
75	-2.32	-2.30	-2.17	-2.24	-2.23	-2.20
50	-2.38	-2.35	-2.32	-2.29	-2.28	-2.25
25	-2.54	-2.54	-2.50	-2.47	-2.47*	-2.44*
15	-2.68	-2.74*	-2.74*	-2.74*	-2.74	-2.74
10	-3.03*	-3.01	-3.00	-2.99	-3.00	-3.02
6	-3.03	-3.13	-3.20	-3.23	-3.29	-3.39
4	-3.03	-3.13	-3.22	-3.29	-3.34	-3.44
2	-3.03	-3.13	-3.23	-3.30	-3.35	-3.45
1	-3.65	-3.65	-3.65	-3.65	-3.65	-3.65

* With this velocity resolution (number of channels) we get the better match for the analytical predictions in thin channels.

squared dispersion, σ^2 , over the box size, L , equals CL^m ; similarly the velocity dispersion squared, δv^2 , over the scale r is Cr^m . Therefore the criteria for a channel to be considered thin, which is $\delta v < \sigma$, translates into

$$N > \frac{\Delta v}{\sigma} \left(\frac{L}{r} \right)^{m/2}. \quad (10)$$

Thus, we do not expect a pure power-law result for a slice of a given width. Indeed, the largest scales of the size of the cube are almost always in a *thin* regime, unless, $N < \frac{\Delta v}{\sigma} \sim 5 - 6$. Figure 2 is consistent with this behaviour.

From Figure 2 we can see that the power spectrum also deviates from the power-law at small scales. For that reason to compare with VCA we have restricted ourselves to the wave number $\log k$ range from ~ 1.3 to ~ 2.2 , where the power spectra in Fig. 2 is close to a power-law. Below, we discuss the causes of the deviations from the power-law behaviour. Using that range in k we calculated the slope (spectral indices) of the power spectra with a linear least-squares method. The measured slopes are shown in Table 2. From Fig. 2 and Table 2 we can see indeed a steepening of the power-spectrum as we increase the thickness of the velocity slices. But the spectral-indices in thin channels don't appear to reach an asymptotic value, instead keep getting shallower as the velocity resolution increases. This behaviour arise due to the limited number of emitters along the LOS. With only 216 emitters along each LOS, to distribute in a large number of velocity channels, there will be many channels empty, rendering in high frequency noise, and making the measured spectrum shallower at larger wave-numbers. As was suggested in Lazarian et al. (2001) it is therefore optimal to search for thin slice asymptotics in the channels that are just thin enough, i.e. $N \approx \frac{\Delta v}{\sigma} \left(\frac{L}{r} \right)^{m/2}$ at the smallest scale r of interest.

The expression in eq. (10) is somewhat tricky, because we need to know the value of m , to get the number of channels to be used to best determine m ! But, it allows to check with emulated observations if the predictions hold. For real observations the problem is alleviated because in that case we are not limited by the number of emitters and we can use the maximum velocity resolution without having empty channels. In Lazarian et al. (2001) the factor of $\Delta v/\sigma$ in eq. (10) was estimated to be ~ 2.5 , in the assumption of Gaussian statistics. To get σ we can take the standard deviation of the velocity along each LOS and average over all the

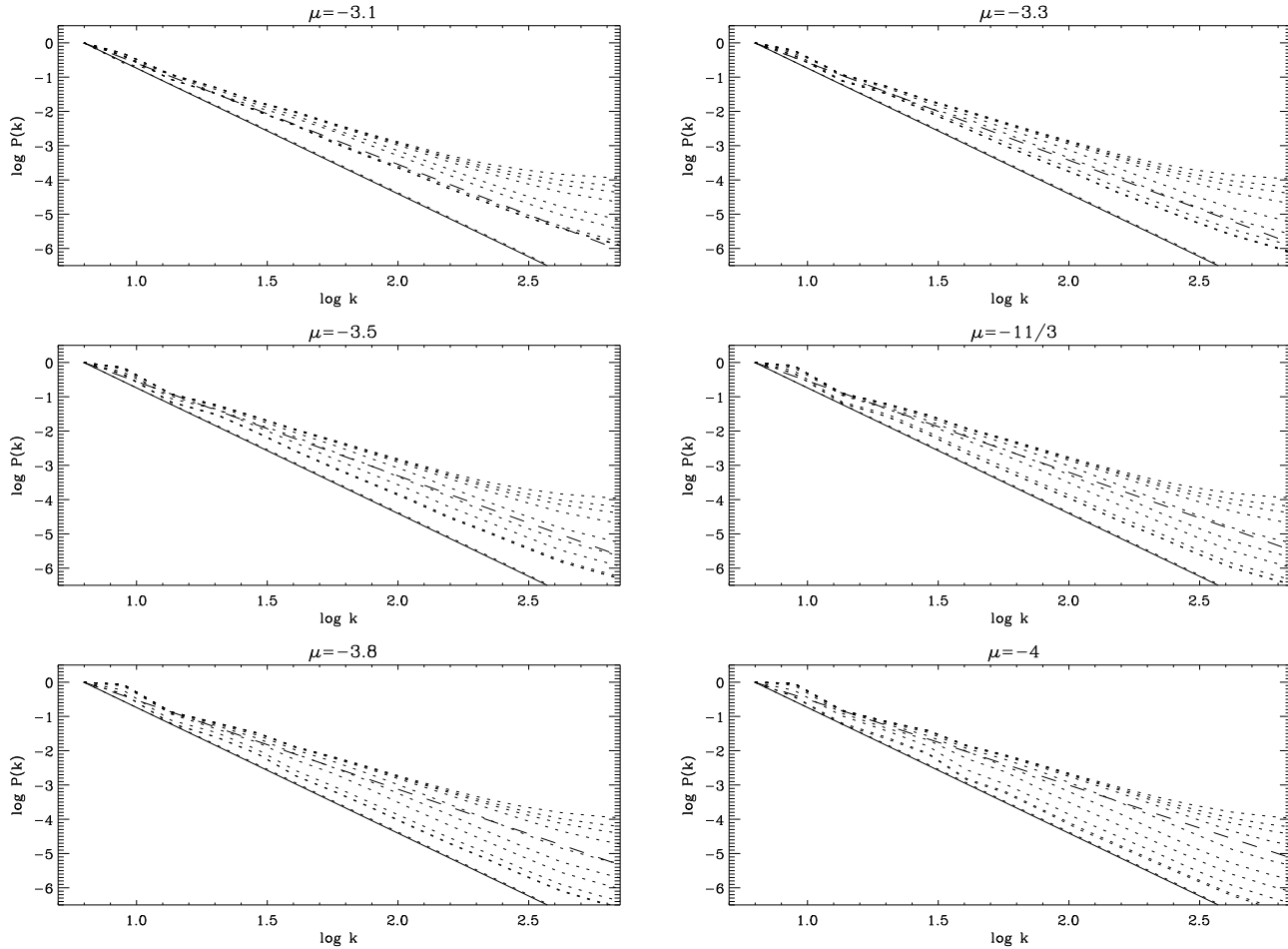


Figure 2. Power spectra in velocity channels for simulated observations with density spectral index of $-11/3$, and various velocity spectral indices (as labelled in the title of each plot). In each panel *dotted* lines correspond to the power-spectra in velocity channels for PPV cubes generated with, top to bottom 150, 100, 75, 50, 25, 15, 10, 6, 4, 2, and 1 channels respectively. For reference we plotted the predictions in LP00: in *dashed* lines are the predictions for thin channels, in *solid* lines for very thick channels.

Table 3. Emissivity spectral indices in barely thin channels

Velocity index	Num. of channels	Predicted γ	Measured γ
-3.1	31	-2.95	-2.49
-3.3	35	-2.85	-2.43
-3.5	39	-2.75	-2.37
-3.67	42	-2.67	-2.32
-3.8	46	-2.6	-2.29
-4.0	54	-2.5	-2.24

LOS available, and Δv is nothing but the range of velocity covered in our PPV cubes. This is important because a side effect of the modification of the spectral index is an appreciable change in the velocity range of the velocity cubes. To get the factor (L/r) we need to take the maximum wave-number used to obtain the power-spectra. For the results presented in Table 2 it was $k \sim 10^{2.2}$, so $L/r = k/2\pi \sim 25$. We generated PPV cubes with the number of channels from from eq. (10), and measure the power spectrum in velocity channels, in Table 3 we display the results. From the table we can see that the measured spectral indices within 20% error of the predictions, but always shallower than expected. This is an in-

ication, that the noise arising from the limited number of emitters is present even in channels barely thin, although not near as large as that present for PPV cubes constructed with more channels (see Table 2).

Could deviations above be due to correlations between the density and the velocity fields? The answer is no: to illustrate that the density velocity correlations of the magnitude found in our simulations are not important to the VCA, we can compare the power spectrum of the MHD simulations to that of an ensemble of 60 synthetic PPV cubes with the same spectral indices. We constructed PPV cubes using the density field from the simulations (modified to spectral index of $-11/3$), with either the modified velocity cube, or Gaussian velocity cubes, both with Komogorov indices. The former have velocity and density correlations similar to those consistent with MHD, the latter are entirely uncorrelated. These power spectra are shown in Fig. 3. In this figure we can appreciate that apart of some ‘wiggles’ at small values of k , due to lack of enough statistics (see discussion below) the power-spectra is practically identical whether the density field is correlated with the velocity field or not.

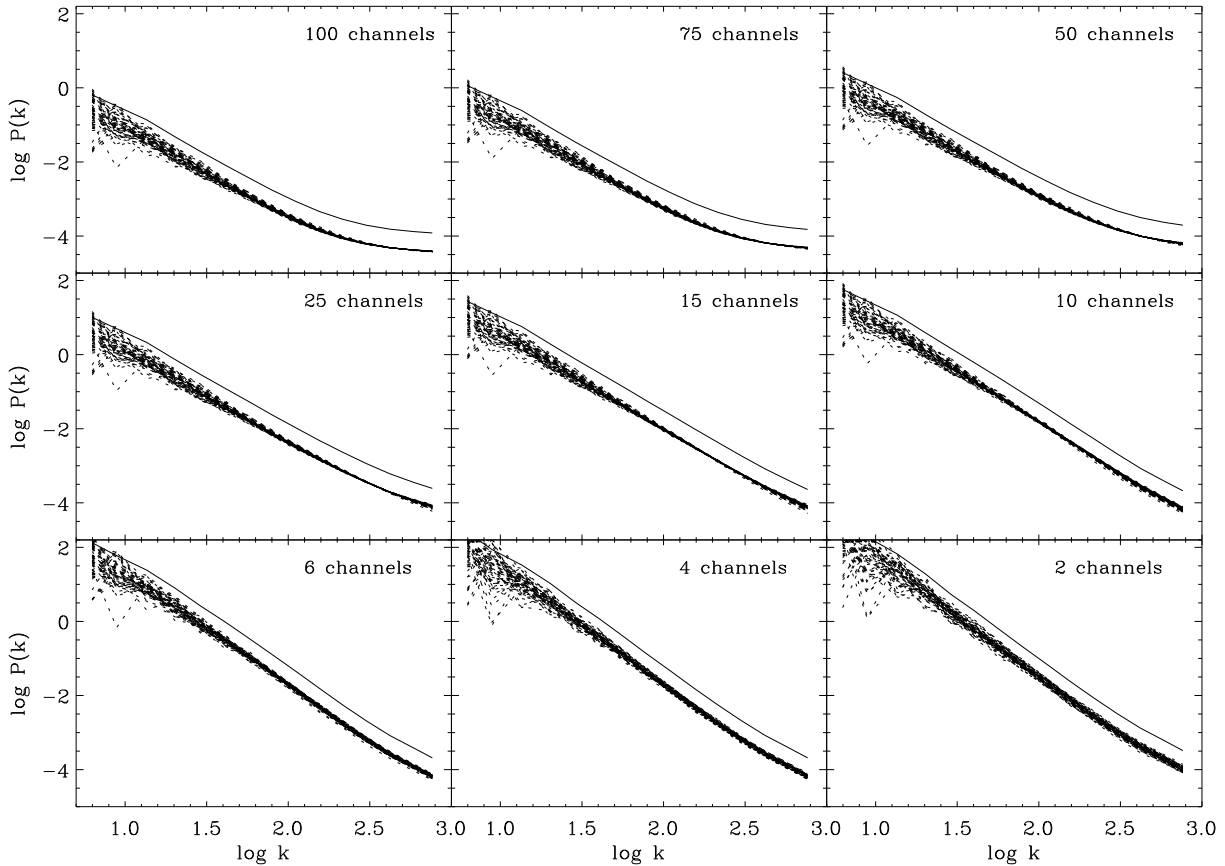


Figure 4. Power spectra in velocity channels for an ensemble of 60 Gaussian cubes of velocity with index $-11/3$ and constant density. The *dotted lines* are the average of the 2D power spectra in velocity channels for individual PPV cubes constructed with the number of channels as denoted in the upper right corner in each plot. The *solid lines* correspond to the ensemble average, and for visual purposes are shifted vertically by 0.5.

3.4 More on the numerical limitations

As we saw in the previous section, one important practical problem with the determination of the spectral indices through VCA is to measure with accuracy the slopes (precisely the spectral indices) in the plots. We can notice from each plot in Fig. 2, two departures from well behaved power-laws. At the left end of the spectrum (low k numbers, large spatial scales) we have some random wiggling, while at the right end of the curves we see a systematic flattening of the power spectrum. The latest is increasingly evident for PPV cubes formed with larger number of channels (with thinner velocity channels), and was referred as ‘shot-noise’ in Lazarian et al. (2001). To explore the nature of those departures from the expectations, and to avoid interference from other sources of uncertainty (i.e. density velocity correlations) we will use simple Gaussian fields with prescribed power-law spectrum as velocity fields and consider a constant density fields to produce PPV cubes (or ‘PV squares’ as we’ll see). We generated an ensemble of 60 Gaussian cubes with spectral index $-11/3$, and produced PPV cubes, with different number of channels (different velocity resolution) assuming a constant density. The power spectra in velocity channels are plotted in Fig. 4. From the figure is evident that the departures from strict power-laws at low k numbers is due to the lack of sufficient statistics at the largest scales: power spectra in velocity channels for individual ve-

locity cubes differ very little from intermediate to large k numbers, but differ significantly at small k , showing some ‘wiggles’. However the ensemble average converges to a power-law that extends from the largest spatial scales to intermediate spatial scales, until the systematic flattening of the power spectrum at large k becomes evident.

The limited number of emitters (density pixels) along the LOS are expected to introduce high frequency (high k) noise in the power to render in a shallower tail, just like that we have observed. This was regarded as ‘shot-noise’, true in the sense that the flattening becomes larger as we increase the velocity resolution, although is more complicated that the usual shot-noise that can be easily described in terms of Poisson statistics. The natural way to get rid of this problem is of course to increase the number of emitters along the LOS. This can be accomplished increasing the size of the data cubes, which translates into more computing power required to analyse the power-spectrum. With the resources at our hand, to extend our range in k we generated an ensemble of 50 2D Gaussian velocity fields of size 1536^2 with spectral indices of $-8/3$ (Kolmogorov in 2D). Analogously to the 3D ensemble we simulated observations and analysed the power spectrum in velocity slices. In Fig. 5 we compare the ensemble average power-spectrum in velocity channels for both, 3D and 2D cases. It’s clear the increase in

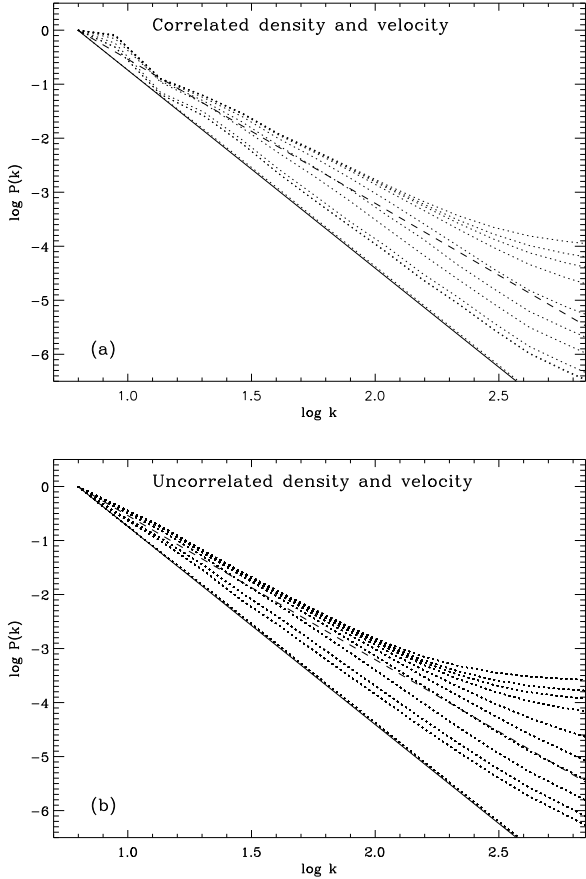


Figure 3. Power spectrum in velocity channels for PPV produced with density and velocity cubes from MHD simulations –with spectral indices modified to $-11/3$ – (a), and with the same density as the left panel but an ensemble of Gaussian cubes with index $-11/3$ (b). The dotted lines correspond to the average spectrum in velocity channels for PPV with different number of channels, in both panels from these correspond from top to bottom to 150, 100, 75, 50, 25, 15, 10, 6, 4, 2, and 1 channels respectively. We see larger departures from power-law behaviour at lower k in (a) because in (b) we averaged over an ensemble, see discussion on the text. Also, in both cases for reference we plotted the predictions of the power spectrum in thick channels (solid lines), and in thin channels (dashed lines).

wave-number range acquired with the 2D data, in which we have about half decade more. The relevant result of this comparison is to show that the flattening of the power spectrum for the thinnest channels is present in both cases, at large k . But for the 3D case this flattening is present earlier than in the 2D case.

It's important to stress that this is NOT a real dynamical effect, the cubes used to construct the PPV cubes are just Gaussian velocity and constant density.

This flattening of the spectrum is particularly problematic precisely because it increases as we go into thinner channels. The predictions in LP00 to extract the velocity spectral index were done in an asymptotic regime for thin channels, and this flattening impede us to use small spatial variations to measure reliably the spectral index for the thinnest channels. Our results, in Table 3, support the prediction in Lazarian et al. (2001) that more channels are required when steeper velocity fields are studied. This shot-like noise presents an obstacle to obtain with high accuracy the velocity index of data cubes generated synthetically. However the

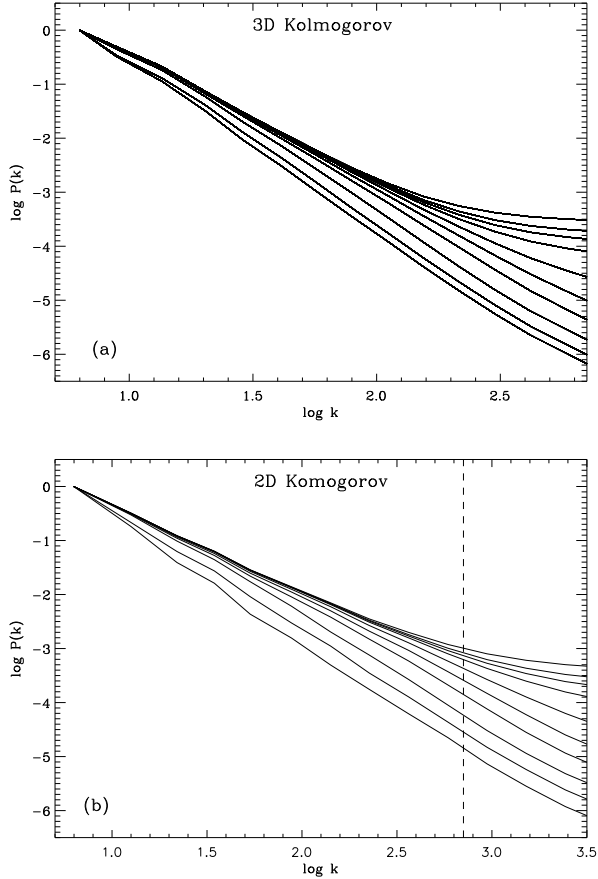


Figure 5. Comparison of the power spectrum in velocity channels for an ensemble of 60 velocity cubes (a) with an ensemble of 50 squares (b). The cubes are 216^3 in size and the squares are 1536^2 . All velocity fields have Kolmogorov spectral indices ($-8/3$ for 2D and $-11/3$ for 3D), and the PPV were obtained with constant density. The dashed line on the right panel is to compare the inertial range achievable in both cases.

problem is not expected to be present in real observations, where the number of emitters along the LOS is much larger, as was confirmed through observations of the Small Magellanic Cloud (Stanimirović & Lazarian 2001). There the spectral indices measured in thinner and thinner channels tend to an asymptotic value, not being affected by shot-like noise, allowing to accurately measure the power-spectrum in velocity channels.

4 ANISOTROPIC TURBULENT CASCADE

Magnetic field plays a crucial role in the dynamics of interstellar turbulence, and makes the turbulent cascade anisotropic (Montgomery 1982; Higdon 1984). In a turbulent magnetized media, the energy on the large scale motions is larger than that on the small scale structures; however the local magnetic field strength remains almost the same. Thus, is easier to bend magnetic field lines on the large scale by turbulent motions, but on the small scale becomes more difficult. Another way to think about this phenomenon is noting that hydrodynamic motions can easily mix magnetic field lines on the small scale, rather than bend them, in the direction perpendicular to the mean magnetic field (see discussion in Lazarian & Vishniac 1999). As a result we get elongated eddies, relative to the

magnetic field that become even more elongated as we go further into smaller scales. A model for incompressible anisotropic turbulence is that of Goldreich & Sridhar (1995). This model has been supported by numerical simulations (Cho & Vishniac 2000; Maron & Goldreich 2001; Cho, Lazarian & Vishniac 2002). Compressible anisotropic MHD turbulence has been studied in (Lithwick & Goldreich 2001) and (Cho & Lazarian 2002).

4.1 Magnetic Field Direction: Anisotropy in Correlation Functions

In an isotropic turbulent cascade correlations depend only on the separation between points. Contours of equal correlation are circular in that case. If on the other hand the turbulence is anisotropic, two point statistics are also anisotropic. In this case contours of iso-correlation become elongated, with symmetry axis given by the magnetic field direction. The technique presented here is similar to one proposed to study magnetic field direction using synchrotron maps (Lazarian 1992). This way, the correlation functions can allow us to determine the direction of the magnetic field. We calculate two point correlation for different 2D maps generated with our data. The correlation function between the two scalar functions $f(\mathbf{x})$ and $g(\mathbf{x})$ can be computed from

$$C(\mathbf{r}) = \frac{\langle (f(\mathbf{x}) - \langle f(\mathbf{x}) \rangle) \cdot (g(\mathbf{x} + \mathbf{r}) - \langle g(\mathbf{x}) \rangle) \rangle}{\sigma_f \sigma_g}, \quad (11)$$

where \mathbf{r} is the separation between two points or ‘lag’, \mathbf{x} is the spatial separation, σ_f and σ_g are the standard deviations of f and g respectively. Here the average is performed on all the radial components and azimuthal angles.

With the original cubes from simulations (no artificial modification of the spectral indices), we calculated the auto-correlation (correlation in eq. (11) with $f(\mathbf{X}) = g(\mathbf{X})$) on various 2D maps: of the integrated intensity (integrated along the LOS, equivalent to a 2D map of column density); of the emissivity at the centroid of the lines, obtained as:

$$j_c(\mathbf{X}) = \frac{\int j(\mathbf{X}) v dv}{\int j(\mathbf{X}) dv}, \quad (12)$$

where the emissivity $j(\mathbf{X})$ in our case is proportional to the first power of the density; and of emissivity in individual velocity channels. Contour maps of iso-correlations calculated of these maps are given in Fig. 6. We can see that anisotropy is present in the contours plotted. It is evident in the case of the emissivity at the centroids of the lines, as well as in the integrated emissivity. In individual velocity slices, we found that the majority of the velocity channels show this anisotropy in the expected direction (elongation of the contours parallel to the mean B field), but in some slices we see the elongation of correlation contours tilted from the mean magnetic field direction. For Fig. 6 we choose a representative slice to illustrate this misleading behaviour.

The main purpose of this subsection was to show an alternative method to obtain the direction of the magnetic field, and also to illustrate that anisotropic cascade is present in our simulations.

The anisotropy based technique could be a unique tool for magnetic field studies, especially when other techniques, e.g. based on dust alignment fail (see Lazarian 2000 for a review on grain alignment).

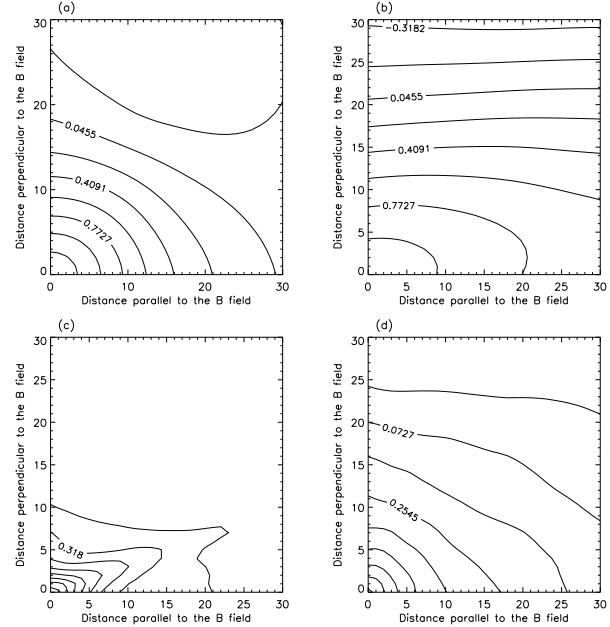


Figure 6. Contours equal correlation of 2D maps obtained with the PPV data. (a): contour map of the correlation of emissivity at the centroid of the lines. (b): contours of correlation in the integrated emissivity. (c), (d): contours in two individual channel maps. This were obtained in a PPV cube with 25 channels (the velocity range is from $V_{min} = -1.27$ to $V_{max} = 1.451$, and consequently the channel thickness is $\delta V = 0.109$). (c) corresponds to a velocity centred at $V_z = -1.11$, while the (d) to a velocity of $V_z = 0.741$. All the distances in the figures are in grid units.

4.2 Anisotropic cascade & VCA.

It’s important to test the VCA, which was developed considering isotropic turbulence, in a more realistic case where the magnetic field determines a preferential direction of the turbulent motions. With that purpose we constructed PPV cubes choosing the LOS to be parallel to the mean magnetic field (along the x axis) and compare the results with the case where the magnetic field is perpendicular to the LOS (z axis). For this exercise we use a data cubes corrected to Kolmogorov spectral indices ($-11/3$ in 3D). The power spectrum in velocity channels is shown in Fig. 7. In the figure we can see that the slopes of the spectrum (spectral index) are almost identical whether the observer is looking parallel or perpendicular to the mean magnetic field. We performed a least-squares linear fitting and found the differences of the slopes in every case are well within the fitting uncertainties.

We conclude that VCA is applicable to anisotropic turbulence studies.

5 EFFECT OF THE SHEAR ON THE VCA

The VCA is sensitive to density and velocity fluctuations at a particular scale. On the other hand, shear as any organized motion, like galactic rotation, would correspond to the smaller wave-numbers (the largest scales, sometimes much larger than the largest scale in a PPV cube), therefore if we choose the right range in k to perform the VCA, we should avoid any interference of this ordered motions with the analysis. To explore numerically the effect of a linear shear on the VCA we used modified data cubes of spectral indices of $-11/3$ for both velocity and density fields. We chose the

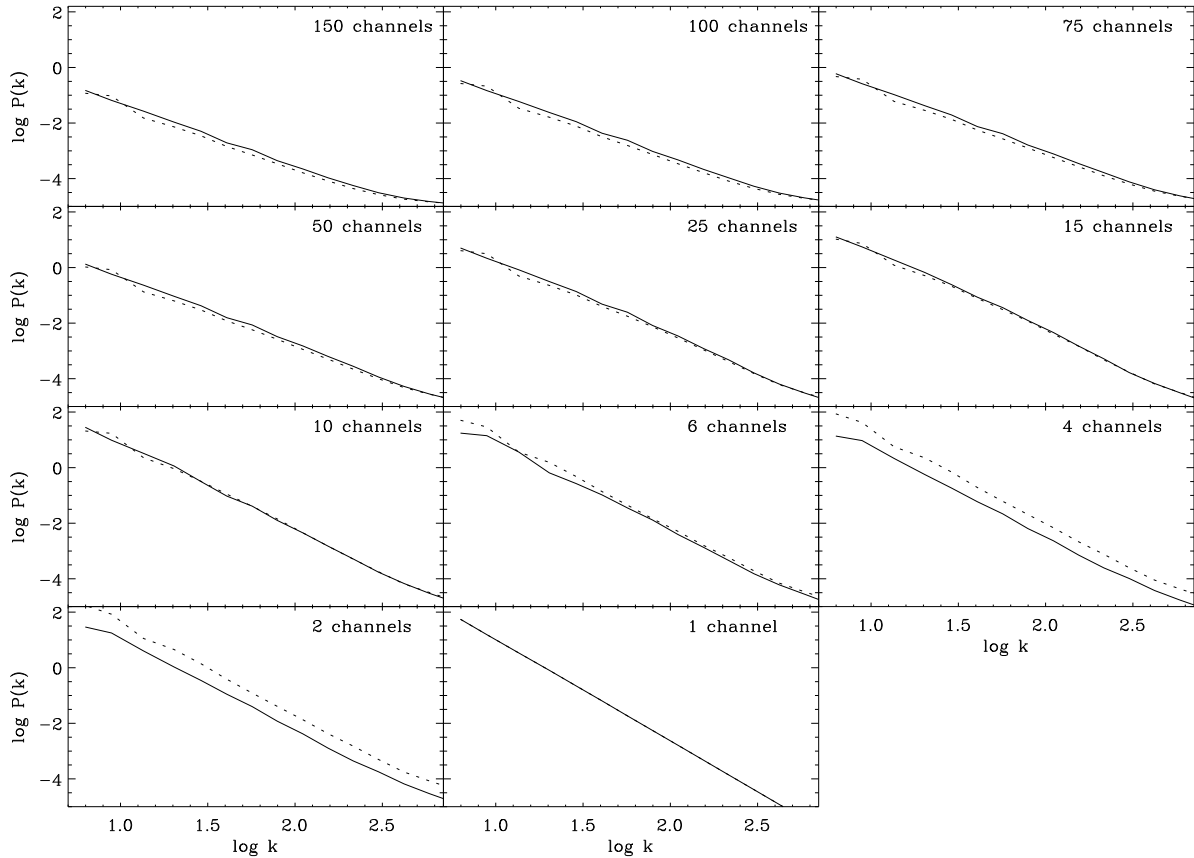


Figure 7. Power spectra in velocity channels for observations with the observer at two different positions. Each panel correspond to the average spectrum in PPV cubes with different number of velocity channels (the number of channels is indicated in the upper right corner on each). The solid lines correspond to the LOS parallel to the mean magnetic field; for the dotted lines the LOS is perpendicular to the mean magnetic field. All the PPV cubes were constructed from the same set of density and velocity data, ‘modified’ to 3D spectral indices of $-11/3$.

LOS to be along the z axis and added a component to the velocity cube (the v_z cube) following:

$$v_z(x, y, z) = v_{0z}(x, y, z) + C\sigma_{v_z} \frac{x}{L} \hat{z}, \quad (13)$$

where v_z is the new velocity cube used to generate the PPV cubes, v_{0z} is the original velocity cube before introducing the shear, σ_{v_z} is the velocity dispersion of v_{0z} , L is the cube size in the spatial coordinates (x, y) , and C is a parameter we introduce to vary the magnitude of the shear introduced. The shear introduced is the same on all scales, and equal in magnitude, to $C\sigma_{v_z}/L$. We generated PPV cubes adding a linear shear with magnitude up to 1, 3, 5, 10, and 20 times maximum velocity dispersion over the largest scale (i.e. with a velocity component with $C = 1, 3, 5, 10$, and 20 in eq. 13). As before, we measure the spectral indices in the range less affected by numerical noise, $\log k$ from ~ 1.3 to ~ 2.2 . The range used is somewhat arbitrary, but the purpose of the study at this point is just comparison with the case of no shear. The measured slopes are summarized in Table 4. The introduced shear is the same on all scales, while the turbulent shear scales as $\sim k^{2/(m-2)}$. It can be shown that the magnitude of the external shear is the same as the magnitude of the turbulent shear when $k \approx 2\pi C^{3/2}$. Therefore the external shear contributed initially to the power spectrum only

Table 4. Spectral indices in velocity channels with shear

Num. of channels	No shear	Shear magnitude (in units of σ_{v_z}/L)				
		1	3	5	10	20
150	-2.2	-2.3	-2.4	-2.4	-2.7	-3.1
100	-2.3	-2.3	-2.4	-2.5	-2.7	-3.1
75	-2.3	-2.4	-2.5	-2.5	-2.8	-3.2
50	-2.4	-2.4	-2.6	-2.6	-2.9	-3.3
25	-2.6	-2.7	-2.8	-2.9	-3.2	-3.7
15	-2.9	-3.0	-3.0	-3.1	-3.4	-4.1
10	-3.2	-3.1	-3.1	-3.3	-3.4	-4.0
6	-3.4	-3.3	-3.1	-3.1	-3.3	-3.7
4	-3.4	-3.3	-3.1	-3.1	-3.3	-3.5
2	-3.4	-3.3	-3.1	-3.1	-3.2	-3.4
1	-3.7	-3.7	-3.7	-3.7	-3.7	-3.7

at the largest scales, but eventually became important at intermediate to small scales as its magnitude increased (see Fig. 8). Our results show that if the maximum shear is less than about 5 times the velocity dispersion over the largest scale, then the relative differences of the spectral indices measured compared with the case of no shear are below 10%, but become larger if the shear increases.

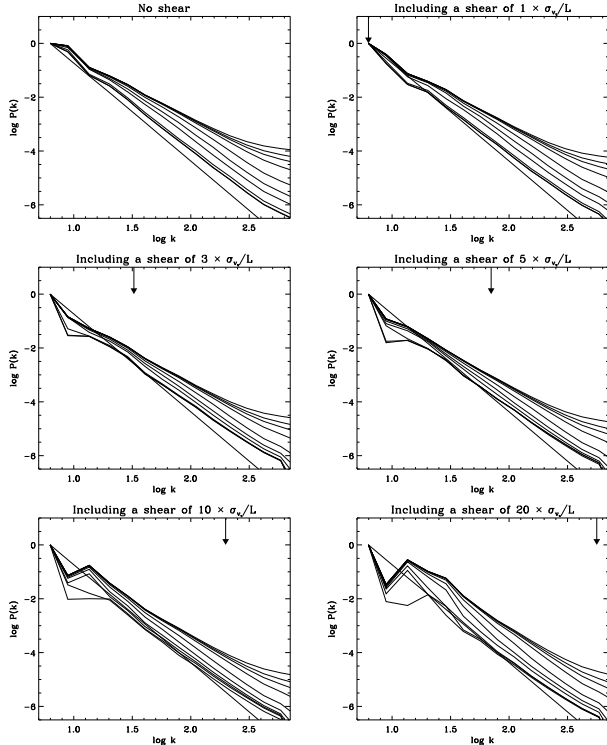


Figure 8. Power spectra in velocity channels including linear shear. Each panel correspond to a different magnitude of the maximum shear, as labelled in the title of each plot. The different lines in each panel correspond from top to bottom to the average power spectrum in velocity channels for PPV cubes constructed with 150, 100, 75, 50, 25, 15, 10, 6, 4, 2, and 1 channels respectively. The small arrows show at which wave-number the magnitude of the external shear equals the magnitude of the turbulent shear.

It is noticeable that the larger distortion due to the introduced shear happens at lower k , even when its magnitude is comparable to the turbulent shear at smaller scales. This is expected, given that the shear is regular, and represents a large scale motion. This holds if we measure the slope of the power spectrum in intermediate spatial scales, which are available using synthetic data. The shear due to turbulence dominates for normal observational circumstances, and its effect is marginal.

6 SUMMARY AND CONCLUSIONS

In this paper we have tested the VCA technique numerically. We have used compressible MHD simulations, and an ensemble of Gaussian fields to emulate spectroscopic observations (PPV data cubes). We computed the power spectra in velocity channels to test the analytical predictions in LP00.

To get the PPV data we modified the output of the simulations to force power-law indices and get a density field (spectral index of $-11/3$), and several velocity fields (with spectral indices from -3.1 to -4.0). The spectral indices derived from our emulated observations are within a 20% error of the analytical predictions. We confirmed trends predicted in LP00, like the steepening of the emissivity index as we increase the width of the velocity channels, or that the velocity fluctuations dominate the emissivity for thin velocity channels is clearly present. This last result is in agreement with a previous result by Pichardo et al. (2000), and is important

because warns observers against interpret any structure in PPV as density enhancements or ‘clouds’ (see also discussion in LP00).

Comparing the results obtained with PPV produced with a constant density and the modified velocity field of spectral index $-11/3$, to those using an ensemble of 60 Gaussian cubes with the same index, we showed that the deviations from power-law behaviour at the largest spatial scales (small k numbers) are due to lack of good statistics at those scales. Another source of error addressed is a flattening of the power spectrum at large wave-numbers. This is due to the limited number of emitters along the LOS. We illustrated this point comparing the results obtained with the ensemble of 60 cubes with 216 emitters along the LOS, and an ensemble with 1536 emitters. Thus, this problem is exclusive of numerical simulations, and is not expected to be important in real observations (like those presented in Stanimirović & Lazarian 2001, where the number of emitting elements is essentially infinite).

We analysed the cross-correlation for 2D maps of integrated intensity and emissivity at the centroids of the lines, and showed that they are anisotropic (elongated), with symmetry axis defined in the direction of the mean magnetic field. This constitutes a new technique to study the direction of the magnetic field. We hope that the anisotropies will reveal the magnetic field within dark clouds, where grain alignment and therefore polarimetry fails. However from the point of view of VCA, we illustrated that the effect of the anisotropy of the turbulence is marginal.

We introduced linear shear to our data, and showed that its effect only becomes important when the magnitude of the shear is more than about 5 times the LOS velocity dispersion. The effect of large scale shear is marginal at small scales. This shows that for ordinary observational situations we can safely neglect shear in the VCA.

ACKNOWLEDGMENTS

AE acknowledges financial support from CONACyT (Mexico). Research by AL is supported by NSF grant AST 01-25544.

REFERENCES

- Brunt C. M., Heyer M. H., 2002a, ApJ, 566, 276
- Brunt C. M., Heyer M. H., 2002b, ApJ, 566, 289
- Cho J., Lazarian A., 2002, Phys. Rev. Lett., 88, 245001
- Cho J., Lazarian A., Vishniac E. T., 2002, ApJ, 564, 291
- Cho J., Vishniac E. T., 2000, ApJ, 539, 273
- Goldreich P., Sridhar S., 1995, ApJ, 438, 763
- Gott J. R., Mellot A. L., Dickinson M., 1986, ApJ, 306, 341
- Bond J. R., Kofman L., Pogosyan D., 1996, Nature, 380, 603
- Heyer M. H., Schloerb F. P., 1997, ApJ, 475, 173
- Higdon J. C., 1984, ApJ, 285, 109
- Jiang G., Wu C., 1999, J. Comp. Phys., 150, 561
- Lazarian A., 1992, Astron. and Astrophys. Transactions, 3, 33
- Lazarian A., 1995, A&A, 293, 507
- Lazarian A., 1999, Plasma Turbulence and Energetic Particles in Astrophysics, Proceedings of the International Conference, Cracow (Poland), 5-10 September 1999, Eds.: Michał Ostrowski, Reinhard Schlickeiser, Obserwatorium Astronomiczne, Uniwersytet Jagielloński, Kraków 1999, p. 28-47., 28
- Lazarian A., 2000, ASP Conf. Ser. 215: Cosmic Evolution and Galaxy Formation: Structure, Interactions, and Feedback, 69
- Lazarian A., Pogosyan D., 2000, ApJ, 537, 72

Lazarian A., Pogosyan D., Vázquez-Semadeni E., Pichardo B., 2001, *ApJ*, 555, 130

Lazarian A., Vishniac E. T., 1999, *ApJ*, 517, 700

Lithwick Y., Goldreich P., 2001, *ApJ*, 562, 279

Liu X., Osher S., 1998, *J. Comp. Phys.*, 141, 1

Maron J., Goldreich P., 2001, *ApJ*, 554, 1175

Mellot A. L., Cohen A. P., Hamilton A. J. S., Gott J. R., Weinberg D. H., 1989, *ApJ*, 345, 618

Miesch M. S., Bally J., 1994, *ApJ*, 429, 645

Monin A. S., Yaglom A. M., *Statistical fluid dynamics: mechanics of turbulence*, Vol. 2., MIT press, Cambridge, MA

Montgomery D., 1982, *Phys. Scripta*, 2, 83

Narayan R., Goodman J., 1989, *MNRAS*, 238, 963

Pichardo B., Vázquez-Semadeni E., Gazol A., Passot, T., Ballesteros-Paredes, J., 2000, *ApJ*, 532, 353

Rosolowsky E. W., Goodman A. A., Wilner D. J., Williams J. P., 1999, *ApJ*, 524, 887

Spangler S. R., Gwinn C. R., 1990, *ApJL*, 353, L29

Scalo J. M., 1987, *ASSL Vol. 134: Interstellar Processes*, 349

Stanimirović S., Lazarian A., 2001, *ApJL*, 551, 53

Scoccimarro R., Couchman H. M. P., Frieman J. A., 1999, *ApJ*, 517, 531